Journal of Alloys and Compounds 509 (2011) 3486–3492

Contents lists available at ScienceDirect

Journal of Alloys and Compounds

journal homepage: www.elsevier.com/locate/jallcom

Temperature impact on morphological evolution of ZnO and its consequent effect on physico-chemical properties

S.B. Kulkarni [a,b], U.M. Patil [a], R.R. Salunkhe [a], S.S. Joshi [b], C.D. Lokhande [a,*]

[a] Thin Film Physics Laboratory, Department of Physics, Shivaji University, Kolhapur, 416 004 MS, India
[b] Rajaram College, Department of Physics, Kolhapur, 416 004 MS, India

ARTICLE INFO

Article history:
Received 12 November 2010
Accepted 6 December 2010
Available online 29 December 2010

Keywords:
Nanocrystalline ZnO
EDTA chelant
Temperature effect
Morphology
Physico-chemical properties

ABSTRACT

The temperature influenced morphology evolution and its effect on physico-chemical properties of ZnO thin films deposited onto glass substrates from alkaline environment, complexed via EDTA chelant are systematically studied. Temperature dependent growth mechanism model for change in microstructure is proposed. The physico-chemical properties of deposited films are studied by the analysis of structural, morphological, surface wettabillity, optical and electrical properties. Nanocrystalline ZnO thin films with hexagonal structure having mari-gold flowers and tetra pods like morphologies with optical band gaps 3.1 and 2.96 eV showed drastic surface wettabillity transformation from highly hydrophobic (142°) to superhydrophilic (<5°) behavior for bath placed at room temperature (300 K) and 333 K, respectively. The room temperature photoluminescence spectrum in the visible light region showed decreasing in intensity and electric resistivity measurement showed reduction in electrical resistivity from 10^6 to 10^4 Ω cm as consequence of increment in deposition temperature. The morphology evolution as impact of bath temperature can provide wide scope with significant change in physico-chemical properties of smart ZnO, which can be potentially tuned in many functional applications with feasibility.

1. Introduction

In recent years, rigorous development in nanotechnology has occurred because of novel optical and electronic properties of nano and micrometer sized materials, which differ from that of bulk materials due to their enhanced surface to volume ratio and quantum confinement effect [1,2]. Control over morphology and crystal size of materials has awakened great interest of researchers in the design of functional devices which decide their feasibility in applications and can be adapted by varying their size and shape [3]. The control of the morphology is a challenging task to develop smart and functional materials.

Zinc oxide (ZnO) has been extensively studied for several years because of its versatility and broad range of applicability in many fields. ZnO is a n-type semiconductor material with direct wide band gap of ~3.3 eV having a large free exciton binding energy of 60 meV, which promotes it as laser material based on exciton recombination at room temperature or even at higher [4]. It has hexagonal (wurtzite type) crystal structure having suitability in the fabrication of high quality oriented or epitaxial thin films. Every zinc atom is tetrahedrally coordinated with four oxygen atoms and zinc '*d*' orbital electrons hybridized with the oxygen '*p*' orbital electrons [5]. The pure ZnO exhibits n-type conductivity, due to the formation of more native donor-type defects i.e. oxygen vacancy (V_O) and Zn interstitial (Zn_i) [6,7]. Electrical conductivity of ZnO is primly due to the presence of surplus zinc at the interstitial position. It possesses diverse range of properties which depend on appropriate doping processes, comprising a varying conductivity from metal to insulator including n-type and p-type [4].

ZnO is one of the most smart functional materials and its structural, morphological, optical, electrical properties in conjunction with wide band gap, excellent chemical and thermal stability put forth it as a strong candidate to fulfill demands in various technological applications such as photoluminescence, transparent semiconductors, photocatalysts, piezoelectric devices, chemical sensors, green-blue-ultraviolet (UV) light emitters, varistors, solar cells, and optoelectronic devices [8,9].

Nowadays, special attention has been focused on the morphological aspect in order to improve the performance of ZnO based materials and to widen their range of applications, because many variety of nanostructures can be grown from ZnO [10]. Various ZnO nanostructures such as nanodots, nanorods, nanowires, nanobelts, nanotubes, nanobridges and nanonails, nanowalls, nanohelixes, seamless nanorings, mesoporous single-crystal nanowires, and polyhedral cages have been reported [11–13]. These nanostructures were grown by different routes such as catalyst-free [14,15] and catalyst-assisted growth [16–20].

* Corresponding author. Tel.: +91 231 2609225.
E-mail address: l.chandrakant@yahoo.com (C.D. Lokhande).

0925-8388/$ – see front matter © 2010 Elsevier B.V. All rights reserved.
doi:10.1016/j.jallcom.2010.12.036

ZnO thin films have been prepared with various thin film deposition techniques, such as pulsed-laser deposition [21], chemical vapor deposition [22], spray pyrolysis [23], chemical bath deposition [4], electrodeposition [24], and hydrothermal [25]. Among them, the chemical bath deposition (CBD) offers the possibility of preparing high quality ZnO thin films on large-area at low temperature and at low cost for technological applications. The CBD method has emerged as an excellent method for the deposition of polycrystalline thin film semiconductors [26]. The key part comprised by CBD method is direct deposition based on heterogeneous nucleation and subsequent crystal growth on substrate surface. The CBD method is mainly used to deposit films of metal chalcogenides or metal oxides by solitary immersion of substrates in aqueous metal ion complexed baths [27].

Any electron donating entity, which has the ability to bind to the metal ion and produce a complex ion can be called as ligand or complexing agent or chelating agent. The ligands which contain more than one group and capable of binding with metal ions are known as multidentate ligands or chelating agents. Usually the solution with a lower supersaturation is favorable for one dimensional growth of the crystals, which can be achieved with use of dilute chelating agents. Westin and Rasmuson reported that the presence of ethylenediaminetetraacetic acid (EDTA) can control the sizes and morphologies of the particles owing to the chelating effects of EDTA with Ca^{2+} and Zn^{2+} [28,29] which can provide a solution with less free metal ions to control the crystals growth by modifying the forms of the aqueous ions. Complexation via EDTA of metal salt in alkaline environment can effectively avoids homogeneous nucleation within the bath due to the binding of metal ions providing priority to heterogeneous nucleation which may be helpful to increase the product yield.

In this paper, ZnO thin films are synthesized at two different temperatures (300 K and 333 K) from an alkaline zinc nitrate solution by adopting EDTA as chelating agent for complexion with good controllability and reproducibility. Also its consequent effect on physico-chemical characteristics such as structural, morphological, wetting, optical and electrical properties of material was systematically studied. In addition, we have proposed the schematic model for the evolution of microstructure as an effect of bath temperature on growth and distribution of the ZnO onto substrate in the thin film form.

2. Experimental

Synthesis of ZnO thin films by CBD method is based on the immersing the substrates into an aqueous alkaline bath of zinc nitrate complexed via multidentate ligand ethylenediaminetetraacetic acid disodium salt (EDTA). Firstly, solution of 0.1 M zinc nitrate as a source of zinc along with 0.05 M EDTA was prepared. Furthermore, aqueous ammonia (NH_4OH) solution (25% extrapure) was added with constant stirring (pH ~ 12). Glass microslides were used as the substrates, which were cleaned with detergent and chromic acid, rinsed with double-distilled water and finally treated with ultrasonic waves for 10 min. The substrates were immersed in the first bath placed at room temperature (300 K). Further to study temperature effect, second bath is kept at 333 K. During precipitation, a heterogeneous reaction occurred and zinc hydroxide was deposited on the substrates. The deposition time required for sample placed at 300 K and 333 K is 3 days and 3 h, respectively. The films were heat treated at 673 K for 2 h, in order to remove hydroxide and to improve the crystallinity of deposited films. The Z1 is annealed sample deposited at bath temperature 300 K and Z2 at 333 K, respectively.

ZnO thin films deposited onto glass substrates were characterized by X-ray diffraction (XRD), Fourier transform infrared (FT-IR) spectroscopy, scanning electron microscopy (SEM) techniques. The thickness measurement of ZnO films was carried out by weight difference method using a sensitive microbalance. Crystallographic and structural study was carried out using Philips PW 3710, X-ray diffractometer (XRD) with chromium radiation ($\lambda = 2.2897$ Å) in the 2θ range from 10° to 100°. The FT-IR spectra of the samples were collected using a 'Perkin Elmer, FTIR Spectrum one' unit. The nanoscale and surface microstructure of the synthesized ZnO were visualized using a JEOL-6360 scanning electron microscope (SEM). The contact angle measurement was carried out using Rame-hart, model 500-F1, USA. The optical properties were investigated using UV–VIS–NIR spectrophotometer, Systronics-119 within the wavelength range 300–900 nm. The room temperature photoluminescence was investigated using Perkin Elmer LS-55 using Xenon excitation source. The electrical properties were studied using two probe resistivity method.

3. Results and discussion

3.1. Film formation

Disodium salt of EDTA ($C_{10}H_{14}N_2Na_2O_8$) is a water soluble chelating agent and is always preferred due to; it is a powerful complexing agent of metals and a highly stable molecule, offering a considerable versatility in industrial and household uses [30]. The chelate wraps around a metal atom to prevent it from oxidizing or early precipitation. EDTA forms complex with most cations. General reaction of complexation between metal ion and H^+ ion for ligand:

$$M^{2+} + [H_2Y]^{2-} \rightarrow [MY]^{2-} + 2H^+ \quad (1a)$$

where 'M' is a metal and $[H_2Y]^{2-}$ is the anion of the disodium EDTA. The schematic model of zinc ion complexation with EDTA chelant is shown in Fig. 1.

The ZnO film formation reaction mechanism can be explained by following equations: Firstly zinc salt in aqueous media reacts with di-sodium salt of EDTA chelant to form zinc–EDTA complex via complexation.

$$Zn(NO_3)_2 + Na_2 \cdot EDTA \rightarrow Zn \cdot EDTA^{-2} + Na_2(NO_3)_2 + 2H^+ \quad (1b)$$

As effect of any external stimulus like temperature or due to hyper time laps the complexed metal ion get released and react with OH^- ions of ammonia to form zinc hydroxide by heterogeneous nucleation.

$$Zn \cdot EDTA^{-2} + 2(NH_4)^{+1} + 2OH^{-1} \rightarrow Zn(OH)_2 + (NH_4)_2 \cdot EDTA^{-2} + 2H^+ \quad (1c)$$

Finally zinc hydroxide is annealed at 673 K for 2 h to form zinc oxide by removal of hydroxide contains and water traces from the deposited samples.

$$Zn(OH)_2 \xrightarrow{673\,K} ZnO + H_2O \quad (1d)$$

3.2. Structural studies

The X-ray diffraction study was carried out for the determination of crystal structure along with structural changes and identification of phases of prepared ZnO thin films. Fig. 2 shows XRD patterns of polycrystalline ZnO on glass substrate, the annealed ZnO samples Z1 deposited at 300 K and Z2 deposited at 333 K, respectively. Table 1 summarizes the observed and standard '*d*' values along with Miller indices, X-ray diffraction intensities with corresponding calculated values of the texture coefficient and lattice parameters for sample Z1 and Z2. By the comparison of observed and standard '*d*' values from JCPDS card number 36-1451, it is concluded that the samples Z1 and Z2 are nanocrystalline and well matched with the hexagonal (wurtzite type) crystal structure having preferred orientation along the (1 0 0) plane. The appearance of small diffraction peaks of (1 0 2), (1 1 0) may ascribe to formation of randomly oriented new crystallites in ZnO film [31]. The average crystallite size of ZnO samples was calculated on the basis of full width at half maxima (FWHM) using Scherrer's formula

$$D = \frac{0.9\lambda}{\beta \cos\theta} \quad (2)$$

where '*D*' is average crystallite size, 'β' is full width at half maxima, 'λ' is wavelength of X-ray used and 'θ' is diffraction angle. The samples Z1 and Z2 have average crystallite size ~20 nm and ~34 nm,

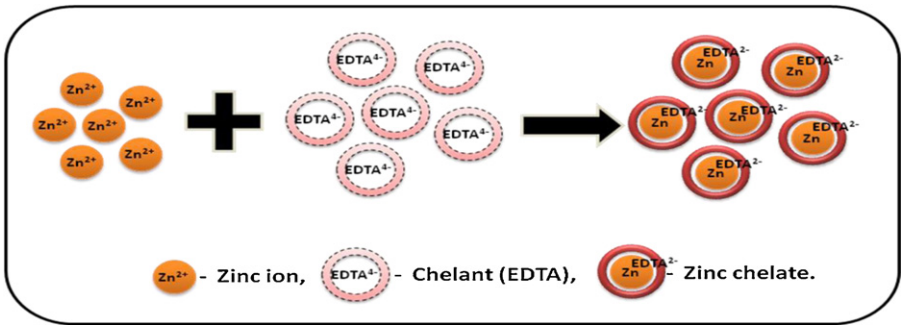

Fig. 1. The schematic model of zinc ion complexation with EDTA chelant.

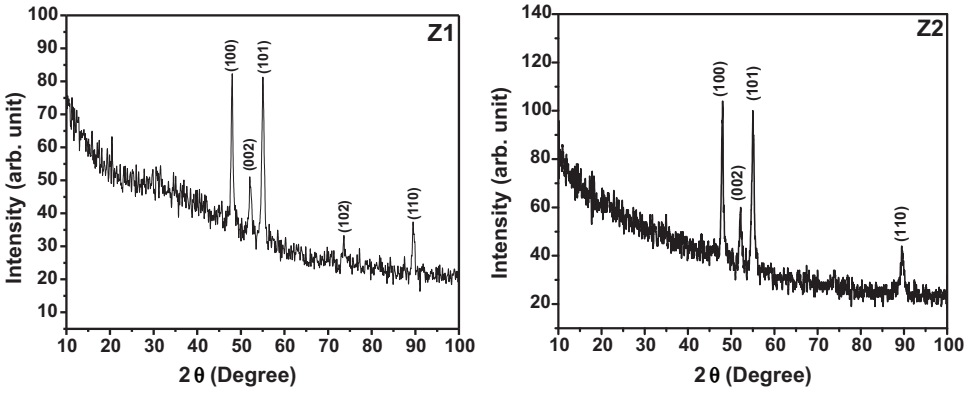

Fig. 2. XRD patterns of the 300 K (Z1) and 333 K deposited (Z2) annealed ZnO thin films.

respectively. The increment in crystallite size can be attributed to the temperature effect at the deposition time.

Furthermore, the amount of the defects in the deposited material was determined by calculating the dislocation density (δ) from the following formula [32]

$$\delta = \frac{1}{D^2} \tag{3}$$

where 'D' is the crystallite size. The smaller value of dislocation densities and larger grains is the indication of the better crystallization. The values of dislocation densities for samples Z1 and Z2 are 2.548×10^{11} cm^{-2} and 0.855×10^{11} cm^{-2}, respectively. This concludes that Z2 sample has better crystallization with less dislocation density than the Z1.

The micro strain is considered as the presence of defects which expands or contracts the nearer lattices by producing local strain close to the defect. The micro strain was calculated by the formula

$$\varepsilon = \frac{\beta \cos\theta}{4} \tag{4}$$

Average grain size, dislocation density, micro strain and thickness of ZnO samples deposited at 300 K and 333 K are tabulated in Table 2. From the observed data, it is revealed that the degree of crystallinity improves with temperature [33] along with decreases in the dislocation density (i.e. imperfection of crystallites) and micro strain. Also reduction in dislocations can be directly correlated with decrease in micro strain in the material.

The reflection intensities from the XRD pattern provide quantitative information regarding the preferred crystallographic orientation in the polycrystalline materials known as texture analysis, which is carried out using the following relationship for the texture coefficient [34].

$$\mathrm{TC}(hkl) = \frac{I(hkl)/I_o(hkl)}{1/N\sum_N I(hkl)/I_o(hkl)} \tag{5}$$

where 'TC(hkl)' is the texture coefficient of the hkl plane, 'I(hkl)' is the standard intensity of the (hkl) plane of sample, 'I_o(hkl)' is the observed intensity of the (hkl) plane and N is the number of diffraction peaks. For a preferentially oriented sample, the texture coefficient TC(hkl) should be greater than one.

From Fig. 3 it is seen that, the value of texture coefficient is greater for index plane (1 0 0) than other planes for both Z1 and Z2 samples, The calculation showed that there is increment in vol-

Table 1
The observed and standard 'd' values along with Miller indices, X-ray diffraction intensities with corresponding values of texture coefficient and lattice parameters of the 300 K (Z1) and 333 K deposited (Z2) annealed ZnO thin films.

'd' values (Å)			hkl	Intensity counts			Texture coefficient TC(hkl)		Lattice parameters (Å)		
Standard	Observed			Standard	Observed				Standard	Observed	
	Z1	Z2			Z1	Z2	Z1	Z2		Z1	Z2
2.8143	2.8153	2.8098	(1 0 0)	57	100	97.8	1.77	1.40	a = 3.2498	3.2508	3.2444
2.6033	2.6028	2.6058	(0 0 2)	44	31.9	41.1	0.73	0.76			
2.4759	2.4750	2.4744	(1 0 1)	100	100	100	1.01	0.81	c = 5.2066	5.2056	5.2116
1.9111	1.9114	–	(1 0 2)	23	13.1	–	0.57	–			
1.6247	1.6245	1.6242	(1 1 0)	32	28.8	39.7	0.91	1.25			

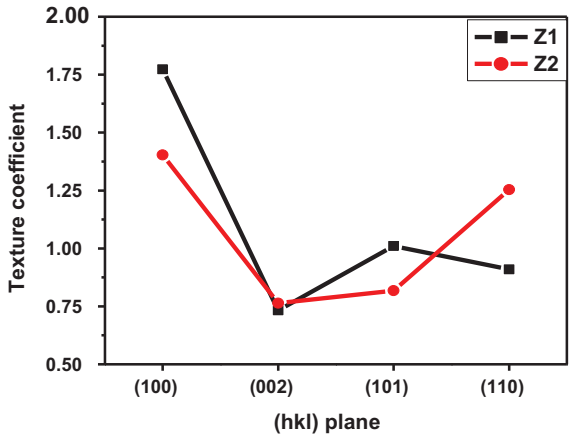

Fig. 3. Texture coefficients for various index planes of the 300 K (Z1) and 333 K deposited (Z2) annealed ZnO thin films.

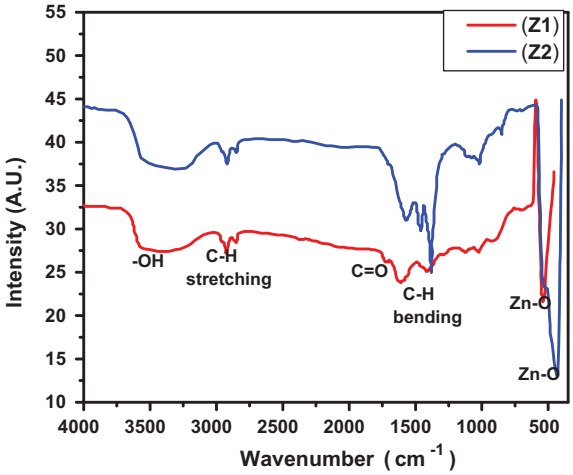

Fig. 4. FT-IR spectrum of the 300 K (Z1) and 333 K deposited (Z2) annealed ZnO thin films.

ume of unit cell for Z1 while, it decreases for Z2 sample as compared to standard data. Also deviation of observed unit cell volume from calculated standard JCPDS data is the indication of the presence of lattice defect or non-stoichiometry of film. Thus variation in relative intensities of the diffraction patterns is due to both crystallographic preferred orientation and lattice defects or deviation from stoichiometry [35].

3.3. FT-IR studies

FT-IR measurement was undertaken in order to confirm the material formation and identify any adsorbed functional groups at the crystals surface as shown in Fig. 4. For sample Z1, the presence of broad band at 3430 cm^{-1} is attributed to surface adsorbed H_2O and –OH group. Peaks at 2919 and 2847 cm^{-1} are ascribed to stretching vibration of C–H bond. The peak observed at 1730 cm^{-1} belong to C=O stretching mode. The bands at 1470–1350 cm^{-1} associate with C–H bond bending. The highly intense peak at 536 cm^{-1} is corresponds to stretching vibration of Zn–O bond [36,37]. While for sample Z2 due to higher bath temperature, shifting of bands at higher wavelength side is observed. The sharp peak at 432 cm^{-1} can be due to the vibration of Zn–O bonding. The shifting of band towards lower frequency side for Z2 is observed due to temperature dependent size effect of the materials as reported in several papers [38]. Herein, the absorption band is significantly red-shifted as compared to that of Z1, showing the increase in average particle size for Z2 sample.

3.4. Surface morphological studies

The morphology of the ZnO samples was revealed by scanning electron microscopy (SEM). Fig. 5a and b shows SEM images of ZnO samples at 5000× magnification as the temperature effect onto the morphological evolution. Nanostructures of mari-gold like and hexagonal shaped tetrapods like morphology can be clearly seen in the magnified views (at 15000×) as Z1′ and Z2′, respectively.

Temperature influenced schematic growth model of ZnO is shown in Fig. 6 supports growth kinetics for morphology alteration. The growth kinetic is slow at room temperature, so two dimensional (2-D) growth of nano species takes place which leads to formation of mari-gold flower like morphology. However, rise in bath temperature results into increase in reaction rate, so ZnO grains rapidly grown, which lead to formation of tetra pod-like morphology comprises bunch of nanorods with random orientations. Also at higher bath temperature breaking rate of complexed metal ions release more metal ions for rapid nucleation and growth process. The morphology evolution of ZnO as influence of bath temperature is due to getting squeezed together of nanodomains into bunch of nanorods to form tetra pod like microstructure. Pawar et al. also reported bath temperature effect onto morphology of ZnO, altered from fibrous flakes into rod like microstructure [39].

3.5. Contact angle

The surface wettabillity study has been of a long standing interest from the point of view of research and commercial applications. The controlling and/or modifying the surface wettabillity of solid surfaces are essential in many situations. Wetting behavior provides the information regarding interaction between liquid and solid in contact and characterized by a microscopic parameter i.e. by measuring the contact angle value. The contact angle is very useful for understanding the material surface properties like wettability, solid surface free energy adhesion, etc. Both the hydrophilic and hydrophobic surfaces have importance in practical appliances [40]. It is well-known that wetting behavior of surface is function of its roughness when characterized by contact angle measurement of material surfaces having identical chemical compositions. Usually, hydrophobicity of surface increases with increase in its roughness.

Fig. 7 shows contact angle measured for sample Z1 and Z2. The surface of ZnO sample grown at 300 K with mari-gold like morphology showed highly hydrophobic nature with a water contact angle of 142°. While, sample grown at 333 K showed superhydrophilic nature with a water contact angle less than 5°, by wetting entire surface. The wettabillity for the samples is found to depend strongly on the surface morphology, which consequences from the growth temperature and is in good agreement with previous

Table 2
Average grain size, dislocation density and micro strain of ZnO samples deposited at 300 K and 333 K.

Bath temperature	Grain size (D) nm	Dislocation density (δ) 10^{11} cm^{-2}	Micro strain (ε) 10^{-3}	Film thickness (t) Å
RT (300 K)	19.81	2.548	2.6026	1087
333 K	34.21	0.855	1.5059	852

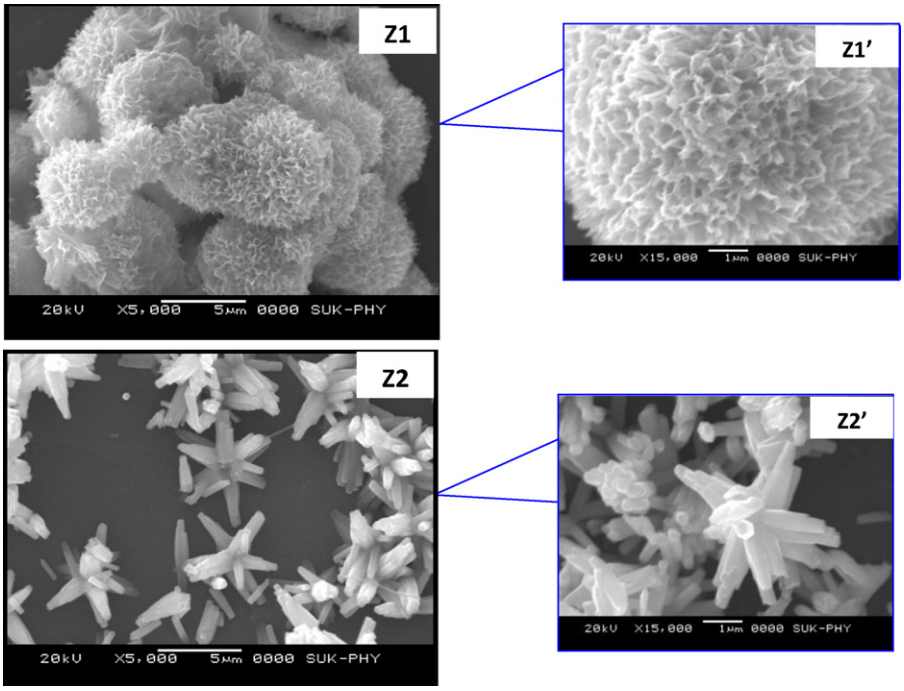

Fig. 5. SEM micrographs of the 300 K (Z1) and 333 K deposited (Z2) annealed ZnO thin films at magnifications 5000× and Z1′, Z2′ are higher magnified images, respectively.

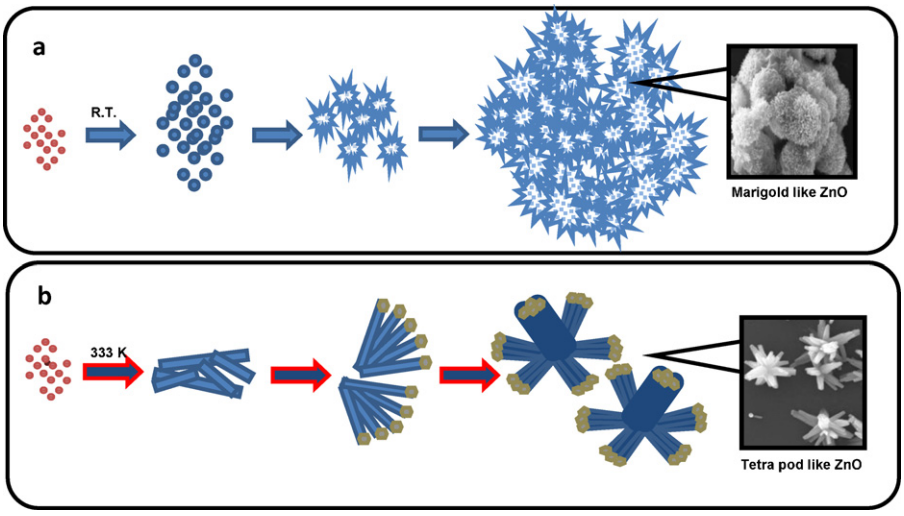

Fig. 6. Temperature influenced schematic growth model of ZnO for sample (a) Z1 and (b) Z2.

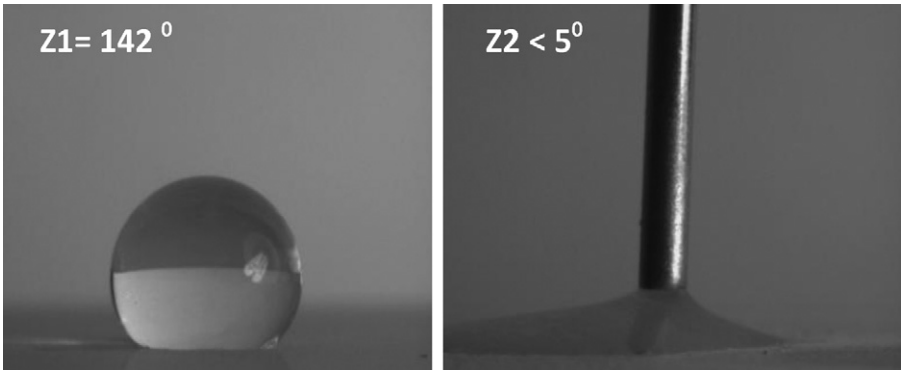

Fig. 7. Water contact angle measurement of the 300 K (Z1) and 333 K deposited (Z2) annealed ZnO thin films.

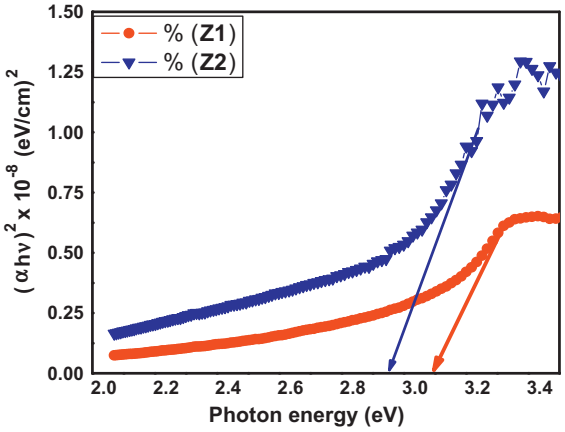

Fig. 8. The variation of $(\alpha h\nu)^2$ versus photon energy $(h\nu)$ of the 300 K (Z1) and 333 K deposited (Z2) annealed ZnO thin films.

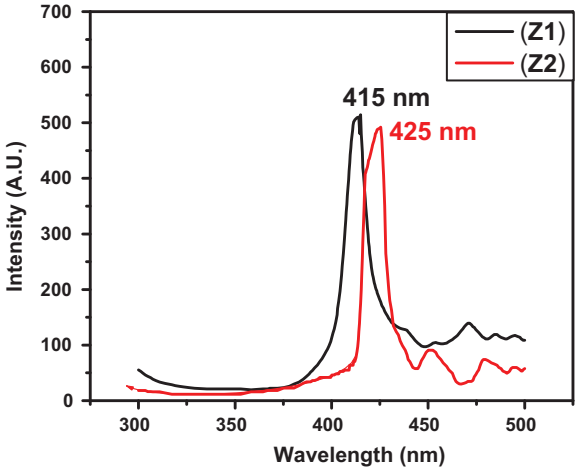

Fig. 9. The room temperature PL spectra of the 300 K (Z1) and 333 K deposited (Z2) annealed ZnO thin films on the glass substrate.

reports [40–42]. The change of wettability may be due to decrease in roughness of sample Z2 than that of Z1. Mari-gold like morphology may provide porous structure with high asperity causes to increase the interfacial surface free energy [43]. However, tetra pods like microstructure may have less roughness resulted into lowering of the interfacial surface free energy showing superhydrophilic behavior.

3.6. Optical properties

Actual information about the optical properties of semiconductors is essential for the design and analysis of various optical and optoelectronic devices. The absorption coefficient (α) with the photon energy $(h\nu)$ has been used to estimate the optical band gap energy of both the samples and is given by Tuac's relation,

$$\alpha = \frac{A(h\nu - Eg)^n}{h\nu} \quad (6)$$

where Eg is the gap between bottom of the conduction band and top of the valence band, $h\nu$ is the photon energy and n is a constant. The value of n depends on the probability of transition; it takes values as 1/2, 3/2, 2 and 3 for direct allowed, direct forbidden, indirect allowed and indirect forbidden transition, respectively. Thus, if plot of $(\alpha h\nu)^2$ versus $(h\nu)$ is linear the transition is direct allowed. Extrapolation, of the straight-line portion to zero absorption coefficient $(\alpha = 0)$, leads to estimation of band gap energy (Eg) values.

The variation of $(\alpha h\nu)^2$ versus photon energy $(h\nu)$ for both the samples is depicted in Fig. 8. The variation of $(\alpha h\nu)^2$ versus $h\nu$ is linear at the absorption edge which confirms that ZnO is semiconductor with direct band gap. The optical band gap (Eg) of sample Z1 is 3.1 eV and it decreases to 2.96 eV for Z2. The decrement in band gap energy can be ascribed to increase in grain size and/or removal of defects due to impact of bath temperature [44]. The decrease in band gap shows that the bath temperature has resulted red shift in the optical absorption [45].

3.7. Photoluminescence

Photoluminescence (PL) technique is appropriate to determine the crystalline quality and impurities in the materials. Fig. 9 depicts room temperature PL spectra for the samples Z1 and Z2 thin films on the glass substrate. Optical properties of the ZnO thin films were investigated by photoluminescence spectroscopy. In the PL spectra of sample Z1 and Z2, several photoluminescence peaks were observed to appear below the photon energy of ~3.0 eV in the visible light region. Herein, sharp photoluminescence peaks are primly recognized in violet light region around photon energy ~3.0 eV. In addition, photoluminescence peaks with lower intensity are found in blue and green light regions around ~2.63–2.74 and ~2.5–2.58 eV, respectively.

The cause of visible photoluminescence in ZnO is still a debatable subject, as various types of extrinsic and intrinsic lattice defects along with different ionization states could be responsible for visible photoluminescence in various emission bands [46]. It is renowned for PL of ZnO that visible emissions at different energies are due to lattice defects of vacancies, interstitials, and antisites. In our case, occurrence of visible photoluminescence pointed out inclusion of different lattice defects in the prepared ZnO samples.

The presence of strong peak around 415 nm in the violet region for the Z1 film can be ascribed to intrinsic defects due to zinc vacancies and interstitials zinc. For Z2 sample as bath temperature increased, the emission was shifted to higher wavelength i.e. ~425 nm. Similar red shift is observed in the optical absorption spectrum which can be attributed to change in the size and shape of the nanocrystals [47]. The weak peaks in the range ~450–500 nm are also found in PL spectrum due to the blue and green emission.

The prominently appeared violet photoluminescence centered at ~2.98 and ~2.91 for Z1 and Z2 samples, respectively, near-band-edge transition of ZnO attributed to an energy loss due to a electron transition from deep donor level of neutral zinc interstitial (Zn_i) to valence band (V_B) [48]. A blue emission at ~2.63 eV can be ascribed to radiative transition of electron from deep donor level of Zn_i to neutral V_{Zn} acceptor level [49]. Moreover, appearance of the blue photoluminescence at ~2.74 is also indication of surface defects present in ZnO samples. The origin of green photoluminescence can be ascribed to radiative transition from deep donor level of Zn_i to acceptor level of singly ionized zinc vacancy V_{Zn}^- [50]. It has been also suggested that the green emission is associated with oxygen deficiency [51].

As bath temperature increases intensity of PL spectra decreases. The weak intensity and red shift in the spectrum corresponds to the evolution in the crystallite size and microstructure. The weak intensity emission spectra of sample Z2 along with less emission peaks compared to Z1 supports increase of crystallite size and decrease of defects/dislocations in the material, which is in well agreement with results from XRD study.

3.8. Electrical resistivity

To understand the variation of electrical resistivity with temperature of ZnO films, two-point d.c. probe method was employed.

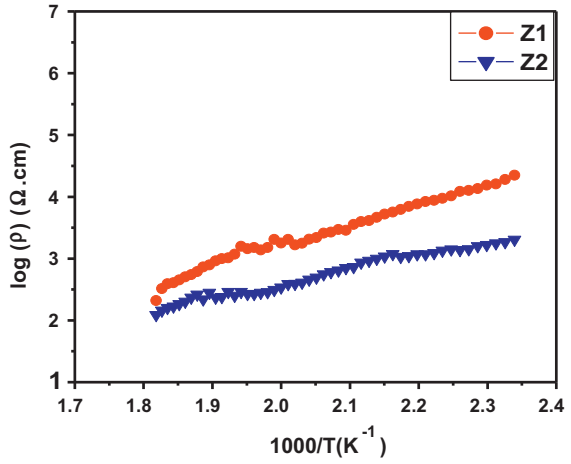

Fig. 10. Plots of log(ρ) versus $10^3/T$ of the 300 K (Z1) and 333 K deposited (Z2) annealed ZnO thin films.

Plots of log(ρ) versus $10^3/T$ for the samples Z1 and Z2 are shown in Fig. 10 indicate the semiconducting nature of the ZnO thin film. The room temperature electrical resistivity was found to be of order of 10^6 Ω cm and 10^4 Ω cm for Z1 and Z2, respectively. The activation energy was calculated using the relation.

$$\rho = \rho_0 \exp\left(\frac{Ea}{kT}\right) \quad (7)$$

where 'ρ' is the resistivity at room temperature T, 'ρ_0' is a constant, 'k' is the Boltzmann constant, and 'Ea' is the activation energy for electrical conduction. It is the amount of thermal energy essential to release an electron from trap level to the conduction band (CB). These trap levels are located in the forbidden region at few meV below the CB and are nothing but the crystal defects [52]. Decrease in the resistivity was found as effect of bath temperature, which is due to increase in crystallite size, as evident from the XRD results. The resistivity is decreased by order 10^2 Ω cm. (Flower like structure have a high specific surface area compared to tetra pods like morphology, but particulate films constructed from small particles have many grain boundaries which diminish the electrical conductivity. Particles should thus have large grain size to decrease grain boundaries and increase electrical conductivity.) The tetra pod like morphology encompasses interconnected nanorods providing channels and is more suitable for the conduction mechanism of electrons rather than porous marry gold like morphology of Z1 sample. The activation energies (Ea) were found to be of the order of 0.71 and 0.45 eV for Z1 and Z2, respectively. These results are also in fever of low resistivity of sample Z2 due to suitability of tetra pods like morphology for conduction mechanism which showed lower activation energy value.

4. Conclusions

The nanocrystalline ZnO films have been successfully deposited from alkaline bath complexed with EDTA chelant. The effect of bath temperature on the crystallinity of the resultant films, microstructures along with distribution onto substrate is explained with help of schematic growth model. The 300 K synthesis inhibits growth reaction rate which resulted into formation of mari-gold flower like structure. The modulation in microstructure observed as result of increase in bath temperature enhances growth rate and promotes the eventual morphology into tetra pods-like nature. Evolution in morphology can eventually alter the physio-chemical properties of ZnO.

Acknowledgement

The authors gratefully acknowledge to the UGC New Delhi (India) for financial support under project file No. 35-16/2008(SR).

References

[1] R. Baron, F.W. Campbell, I. Streeter, L. Xiao, R.G. Compton, Int. J. Electrochem. Sci. 3 (2008) 556.
[2] A.B. Moghaddam, M. Kazemzad, M.R. Nabid, H.H. Dabaghi, Int. J. Electrochem. Sci. 3 (2008) 291.
[3] D.J. Milliron, S.M. Hughes, Y. Cui, L. Manna, J. Li, L.W. Wang, A.P. Alivisatos, Nature 430 (2004) 190.
[4] S.M. Lukas, L. Judith, D. MacManus, Mater. Today 10 (2007) 40.
[5] N. Tamaki, A. Onodera, T. Sawada, H. Yamashita, J. Kor. Phys. Soc. 29 (1996) S668.
[6] S.B. Zhang, S.H. Wei, A. Zunger, Phys. Rev. B 63 (2001) 075205.
[7] H.S. Kang, J.S. Kang, J.W. Kim, S.Y. Lee, J. Appl. Phys. 95 (2004) 1246.
[8] V.R. Shinde, T.P. Gujar, C.D. Lokhande, R.S. Mane, S.H. Han, Mater. Sci. Eng. B 137 (2007) 119.
[9] X.D. Gao, X.M. Li, J. Mater. Res. 22 (2007) 1815.
[10] L. Vayssieres, K. Keis, A. Hagfeldt, S.E. Lindquist, Chem. Mater. 13 (2001) 4395.
[11] Z.L. Wang, Mater. Today 7 (2004) 26.
[12] J.H. Park, H.J. Choi, Y.J. Choi, S.H. Sohn, J.G. Park, J. Mater. Chem. 14 (2004) 35.
[13] J.H. Park, H.J. Choi, J.G. Park, J. Cryst. Growth 263 (2004) 237.
[14] W.I. Park, D.H. Kim, S.W. Jung, G.C. Yi, Appl. Phys. Lett. 80 (2002) 4232.
[15] W.I. Park, G.C. Yi, M.Y. Kim, S.J. Pennycook, Adv. Mater. 14 (2002) 1841.
[16] Y.W. Wang, L.D. Zhang, G.Z. Wang, X.S. Peng, Z.Q. Chu, C.H. Liang, J. Cryst. Growth 234 (2002) 171.
[17] P.D. Yang, H.Q. Yan, S. Mao, R. Russo, J. Johnson, R. Saykally, N. Morris, J. Pham, R.R. He, H.J. Choi, Adv. Funct. Mater. 12 (2002) 323.
[18] S.Y. Li, C.Y. Lee, T.Y. Tseng, J. Cryst. Growth 247 (2003) 357.
[19] Y. Ding, P.X. Gao, Z.L. Wang, J. Am. Chem. Soc. 126 (2004) 2066.
[20] M.H. Huang, Y.Y. Wu, H. Feick, N. Tran, E. Weber, P.D. Yang, Adv. Mater. 13 (2001) 113.
[21] Y. Sun, G.M. Fuge, M.N.R. Ashfold, Chem. Phys. Lett. 396 (2004) 21.
[22] Y. Li, G.W. Meng, L.D. Zhang, F. Phillipp, Appl. Phys. Lett. 76 (2000) 2011.
[23] V.R. shinde, T.P. Gujar, C.D. Lokhande, Sens. Actuators B 120 (2007) 551.
[24] A.I. Inamdar, S.H. Mujawar, S.R. Barman, P.N. Bhosale, P.S. Patil, Semicond. Sci. Technol. 23 (2008) 085013.
[25] L. Wuand, Y. Wu, J. Mater. Sci. 42 (2007) 406.
[26] S. Nizam, A. Rahman, A. Shafii, A.F.M. Nor, B. Kamaluddir, J. Solid State Sci. Technol. Lett. 9 (2002) 354.
[27] K. Kakiuchi, E. Hosono, T. Kimura, H. Imai, S. Fujihara, J. Sol Gel Sci. Technol. 39 (2006) 63.
[28] K.J. Westin, A.C. Rasmuson, J. Colloid. Interface Sci. 282 (2005) 370.
[29] K.J. Westin, A.C. Rasmuson, J. Colloid. Interface Sci. 282 (2005) 359.
[30] D. Williams, Chem. Br. 1 (1998) 48.
[31] M. Izaki, J. Elctrochem. Soc. 146 (1999) 4517.
[32] X.S. Wang, Z.C. Wu, J.F. Webb, Z.G. Liu, Appl. Phys. A 77 (2003) 561.
[33] K. Ramamoorthy, M. Arivanandhan, K. Sankarnarayanan, C. Sanjeevaraja, Mater. Chem. Phys. 85 (2004) 257.
[34] C.S. Barrett, T.B. Massalski, Structure of Metals, Pergamon Press, Oxford, 1980, p. 204 (Chapter 9).
[35] A.A. Ramadan, A.A. E-Mongy, A.M. E-Shabiny, A.T. Mater, S.H. Mostafa, E.A. E-Sheheedy, H.M. Hashem, Cryst. Res. Technol. 44 (2009) 111.
[36] S.J. Jun, S. Kim, J.H. Han, J. Kor. Ceram. Soc. 35 (1998) 209.
[37] A.C. Tas, P.J. Majewski, F. Aldinger, J. Am. Ceram. Soc. 83 (2000) 2954.
[38] H.C. Choi, Y.M. Jung, S.B. Kim, Vib. Spectrosc. 37 (2005) 33.
[39] S.M. Pawar, K.V. Gurav, S.W. Shin, D.S. Choi, I.K. Kim, C.D. Lokhande, J.I. Rhee, J.H. Kim, J. Nanosci. Nanotechnol. 10 (2010) 3412.
[40] R.D. Sun, A. Nakajima, A. Fujishima, T. Watanabe, K. Hashimoto, J. Phys. Chem. B 105 (2001) 1984.
[41] T. Dedova, J. Klauson, C. Badre, Th. Pauporté, R. Nisumaa, A. Mere, O. Volobujeva, M. Krunks, Phys. Status Solidi 205 (2008) 2355.
[42] B. Bhushan, K. Koch, Y.C. Jung, Appl. Phys. Lett. 93 (2008) 093101.
[43] A.B.D. Cassie, S. Baxter, Trans. Faraday Soc. 40 (1944) 546.
[44] K.G. Kanade, B.B. Kale, R.C. Aiyer, B.K. Das, Mater. Res. Bull. 41 (2006) 590.
[45] S.T. Tan, B.J. Chen, X.W. Sun, W.J. Ean, H.S. Kwok, X.H. Zhang, S.J. Chssua, J. Appl. Phys. 98 (2005) 013505.
[46] K.H. Tam, C.K. Cheung, Y.H. Leung, A.B. Djurisic, C.C. Ling, C.D. Beling, S. Fung, W.M. Kwok, W.K. Chan, D.L. Phillips, L. Ding, W.K. Ge, J. Phys. Chem. B 110 (2006) 20865.
[47] A.B. Djurisic, Y.H. Leung, Small 944 (2006) 8.
[48] X.M. Fan, J.S. Lian, L. Zhao, Y. Liu, Appl. Surf. Sci. 252 (2005) 420.
[49] T. Tatsumi, M. Fujita, N. Kawamoto, M. Sasajima, Y. Horikoshi, Jpn. J. Appl. Phys. 43 (2004) 2602.
[50] Q.X. Zhao, P. Klason, M. Willander, H.M. Zhong, W. Lu, J.H. Yang, Appl. Phys. Lett. 87 (2005) 211912.
[51] A. Teke, U. Ozgu¨r, S. Dog˘an, X. Gu, H. Morkoc, B. Nemeth, J. Nause, H.O. Everitt, Phys. Rev. B 70 (2004) 195207.
[52] V.R. Shinde, C.D. Lokhande, R.S. Mane, S.H. Han, Appl. Surf. Sci. 245 (2005) 407.